

Integration of Functional MRI and White Matter Tractography in CyberKnife Radiosurgery

Technology in Cancer Research & Treatment
2017, Vol. 16(6) 850–856
© The Author(s) 2017
Reprints and permission:
sagepub.com/journalsPermissions.nav
DOI: 10.1177/1533034617705283
journals.sagepub.com/home/tct


Lu Sun, MM¹, Baolin Qu, MD², Jinyuan Wang, MM², Zhongjian Ju, MD², Zizhong Zhang, MM¹, Zhiqiang Cui, MD¹, Yang Jack, PhD³, Zhipei Ling, MD¹, Xinguang Yu, MD¹, and Longsheng Pan, MD¹

Abstract

Purpose: To investigate the efficacy of the integration of functional magnetic resonance imaging and diffusion-tensor imaging tractography data into CyberKnife radiosurgery for intracranial tumor management. **Materials and Methods:** Functional neuroimaging, anatomical magnetic resonance imaging, and computed tomography images of patients with brain lesions in critical areas were acquired before radiosurgery. The acquired data sets were coregistered using the MIM image fusion software module and then were imported into the CyberKnife Robotic Radiosurgery System (Multiplan 4.0.2) for delineating the target, organs at risk, and possible nearby functionally relevant cortical and subcortical areas. Radiation dose distributions with and without the functionally relevant cortical and subcortical areas into the optimization process were developed and compared. **Results:** There were significant differences between the treatment plans with and without the functionally relevant cortical and subcortical areas into the optimization process. An average 22.71% reduction in the maximum dose to functional areas was observed. No neurological complication due to radiation damage was observed in the follow-up period. **Conclusion:** The functional neuroimaging could be easily and reliably integrated into the CyberKnife treatment planning. Consideration of functional structures and fiber tracts during treatment planning could clinically reduce the radiation doses to these critical structures, thereby preserving its unique function of brain.

Keywords

CyberKnife, stereotactic radiotherapy, diffusion tensor imaging, white matter, head and neck cancer

Abbreviations

AVM, arteriovenous malformation; BOLD, blood oxygenation level dependent; CI, conformity index; CT, computed tomography; 3-D, 3-dimensional; DTI, diffusion tensor imaging; fMRI, functional magnetic resonance imaging; HI, homogeneity index; MRI, magnetic resonance imaging; MU, monitor unit; NCFs, neurocognitive functions; nCI, new CI; OARs, organs at risk; SRS, stereotactic radiosurgery; VOI, volume of interest

Received: April 19, 2016; Revised: February 28, 2017; Accepted: March 24, 2017.

Introduction

Stereotactic radiosurgery (SRS) has been used either alone or combined with other therapeutic methods to manage various intracranial lesions and has been proved to be a safe, effective therapy.¹⁻³ Despite its noninvasive nature, complications due to radiation should not be overlooked, especially the brain lesions located in critical areas. It is reported that risk of radiation complications will reach 3% if the lesion located in the motor

¹ Department of Neurosurgery, PLA General Hospital, Beijing, China

² Department of Radiation Oncology, PLA General Hospital, Beijing, China

³ Department of Radiation Oncology, Monmouth Medical Center, Long Branch, NJ, USA

Corresponding Author:

Longsheng Pan, MD, Department of Neurosurgery, PLA General Hospital, Fuxing Road Yard 28, Beijing 100853, China.
Email: panls301@163.com



cortex is treated.⁴ This risk is much higher when lesions are located in the thalamus, basal ganglia, or brain stem.⁵⁻⁷ Efficacy of radiosurgery treatment and complications largely depends on the quality of neuroimaging. In general, the target and organs at risk (OARs) were delineated using computed tomography (CT)/anatomical magnetic resonance imaging (MRI) images. When the lesions located within critical areas, functional structures and white matter pathways near the lesions, such as pyramidal tract, arcuate fasciculus, optic tract, Broca's area, Wernicke's area, and so on, are likely to receive a radiation dose beyond their tolerable limit, because they can't be easily identified on CT/anatomical MRI images. Functional neuroimaging, including blood oxygenation level-dependent (BOLD) and diffusion tensor imaging (DTI) tractography, can identify the location of functional structures and white matter pathways; moreover, abnormalities of white matter tracts could be identified. These imaging techniques have been used to guide neurosurgeons to remove critically located intracranial lesions, while protecting nearby function regions.⁸⁻¹⁰ For the same reason, these imaging techniques could and should be implemented in radiotherapy planning system and used to decrease the radiation dose that nearby critical cortical and subcortical areas received by avoiding beams direction passing through them during treatment planning.

The CyberKnife (Accuray, Sunnyvale, California) is a new system for SRS. It uses real-time, noninvasive, image-guidance system, which can ensure the accuracy of localization. The frameless feature can alleviate the patient's distress to some extent. And its original skull-tracking system ensures it has natural advantage in the treatment of intracranial tumors.¹¹⁻¹³ The purpose of this article was to investigate the efficacy of the integration of functional MRI (fMRI) and DTI tractography data into CyberKnife radiosurgery. Radiation dose distributions with and without the functionally relevant cortical and subcortical areas into the optimization process were developed and compared.

Materials and Methods

Patients

We retrospectively reviewed the database of 16 patients who had undergone CyberKnife to treat brain lesions in critical areas from December 2013 to June 2015. The lesions included 2 meningioma, 8 brain metastases, and 6 arteriovenous malformation (AVM). The median age of the patients was 51.5 years (range: 23-76 years). Seven patients were female and 9 were male. All of the patients underwent functional neuroimaging as well as anatomical MRI and CT for CyberKnife radiosurgery treatment plans. The median prescription dose to the tumor was 21 Gy (range: 14-22.5 Gy), delivered in a median of 3 fractions (range: 1-3 fractions). The patients' characteristics are shown in Table 1, and information about pathological type, prescription dose/fraction, and number/size of collimators of all cases is shown in Table 2.

Table 1. The Characteristics of the Patients.^a

| Characteristics | Number of Patients |
|----------------------------------|---------------------------|
| Median age | 51.5 (range: 23-76 years) |
| Gender (male/female) | 9/7 |
| Median prescription dose | 21 (range: 14-22.5 Gy) |
| Median fractions | 3 (range: 1-3) |
| Lesion location | |
| Frontal lobe (left/right) | 8 (5/3) |
| Parietal lobe (left/right) | 6 (2/4) |
| Basal ganglia (left/right) | 2 (1/1) |
| Pathological type | |
| Brain metastases | 8 |
| Primary tumor | |
| Pulmonary adenocarcinoma | 6 |
| Thyroid papillary adenocarcinoma | 1 |
| Renal clear cell carcinoma | 1 |
| Arteriovenous malformation (AVM) | 6 |
| Meningioma | 2 |

^aCharacteristics of the studied patients; 1 Gy = 100 cGy.

Imaging and Delineation of Targets and Critical Structures

Noncontrast axial CT images (120 kV; 320 mA; 27 cm field of view; 1-mm slice thickness; 512 × 512 matrix) were acquired using a 64-multislice CT scanner (Siemens Sensation 16; Siemens, Erlangen, Germany). And the corresponding anatomical MRI data sets (repetition time, 1650 milliseconds, echo time, 4.19 milliseconds; 260 × 260 matrix; 1-mm slice thickness) were also acquired using a 1.5 T Magnetic Resonance Imaging (MRI) scanner (Siemens Espree, Erlangen, Germany). The enhanced T1-weighted imaging (T1WI) was acquired after patients received an injection of gadolinium-diethylenethiamine pentaacetic acid at a dosage of 0.2 mmol/kg. The enhanced T1WI was performed with the following parameters: repetition time, 1650 milliseconds, echo time, 4.19 milliseconds; matrix, 260 × 260; 1-mm slice thickness.

To get the DTI, we applied a single-shot spin-echo diffusion-weighted echo planar imaging sequence (echo time, 147 milliseconds; repetition time, 9400 milliseconds; matrix size, 128 × 128; field of view, 251 × 251 mm; slice thickness, 3 mm; bandwidth, 1502 Hz per pixel; diffusion-encoding gradients in 12 directions using *b* values of 0 and 1000 s/mm²; and voxel size, 1.9 × 1.9 × 3 mm³). We used 40 slices, no intersection gap, 40 continuous free interval collection slices, and 5 time repetitions. To image the eloquent cortex, we used a block design composed of stimulation and rest. The hand and foot movement tasks were used to map functional areas specialized in hand and foot movements.

For fiber tracking, we used the "fiber tracking" module of i-plan software (version 3.0; Brain Lab Inc, Munich, Germany) to reconstruct the corticospinal pathway and the sensory pathway. We used a multi-volume of interest (VOI) algorithm for fiber tracking, and the tracking was performed by defining a rectangular VOI in the coregistered standard T1 anatomical data sets. After selecting the appropriate fiber bundle, a

Table 2. Information About Pathological Type, Prescription Dose/Fraction, and Number/Size of Collimators.

| Pt No | Pathological Type | Prescription Dose, Gy | Fractions | Number/Size of Collimators |
|-------|--|-----------------------|-----------|----------------------------|
| 1 | Brain metastases of thyroid cancer | 13 | 1 | 2/5 mm; 10 mm |
| 2 | AVM | 16 | 1 | 2/12.5 mm; 20 mm |
| 3 | AVM | 14 | 1 | 3/5 mm; 10 mm; 20 mm |
| 4 | AVM | 15 | 1 | 2/5 mm; 10 mm |
| 5 | AVM | 15 | 1 | 2/7.5 mm; 12.5 mm |
| 6 | Meningioma | 21 | 3 | 2/15 mm; 30 mm |
| 7 | Brain metastases of lung cancer | 21 | 3 | 2/12.5 mm; 25 mm |
| 8 | Meningioma | 21 | 3 | 2/7.5 mm; 20 mm |
| 9 | Brain metastases of renal clear cell carcinoma | 21 | 3 | 2/10 mm; 15 mm |
| 10 | Brain metastases of lung cancer | 19.5 | 3 | 2/12.5 mm; 20 mm |
| 11 | Brain metastases of lung cancer | 21 | 3 | 2/5 mm; 10 mm |
| 12 | Brain metastases of lung cancer | 21 | 3 | 2/7.5 mm; 15 mm |
| 13 | Brain metastases of lung cancer | 21 | 3 | 2/10 mm; 20 mm |
| 14 | AVM | 22.5 | 3 | 2/12.5 mm; 20 mm |
| 15 | Brain metastases of lung cancer | 22.5 | 3 | 2/15 mm; 25 mm |
| 16 | AVM | 21 | 3 | 3/10 mm; 25 mm; 40 mm |

Abbreviations: AVM, arteriovenous malformation; Pt No, patient number.

3-dimensional (3-D) object was created automatically by wrapping the neighboring fibers with a hull. Methods of DTI and BOLD fMRI acquisitions have been described elsewhere.¹⁴

The data sets of fMRI and DTI were fused with the corresponding anatomical MRI and then registered with CT images using the MIM image fusion software (version 6.5.4; MIM Software Inc, Cleveland, Ohio). The fused DICOM images were then imported onto the CyberKnife robotic radiosurgery system for delineating target volumes, OARs, and nearby functionally relevant cortical and nearby subcortical areas. Figure 1 showed the CT of patients with intracranial metastatic tumor, DTI data sets overlaid on the anatomical MRI, and the CT fused with the anatomical MRI as well as DTI data sets. Using CT/anatomical MRI images, the targets, and standard OARs including brain stem, bilateral optic nerves, eyes, and optic chiasm were delineated. The functional structures of the brain and the fiber tracts nearby the targets were also contoured as additional OARs using the fused fMRI and DTI images.

Treatment Planning

We developed 2 treatment plans for each case using the sequential optimization tool of the CyberKnife robotic radiosurgery system. In the first one, only the target and standard OARs were considered in the optimization process. In the other, the functional structures and fiber tracts were added to the optimization process as additional OARs, which were treated in the same way as the standard OARs. In the both plans, target coverage was always optimized first to ensure maximum therapeutic benefit, and the second is the maximum and average allowed doses to be delivered to the standard OARs. Meanwhile, to ensure the comparability of the dose to functional areas in the 2 plans, we sought to achieve the same prescription dose to the target for each case. The collimator dimension was selected according to the volume and shape of the target. The maximum number of monitor units (MUs) of each beam is depended on

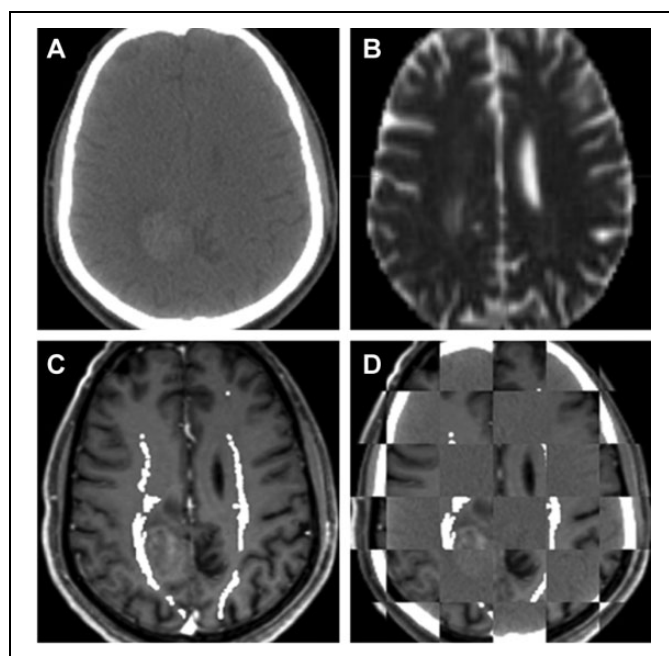


Figure 1. (A) Acquired axial CT, (B) original DTI, (C) DTI data sets fused with the corresponding anatomical MRI. D, The fused MRI registered with CT scan from the patient with intracranial metastatic tumor. DTI fused with the anatomical MRI data showing the pyramidal tracts. CT indicates computed tomography; DTI, diffusion tensor imaging; MRI, magnetic resonance imaging.

the volume of the target, the distance from the additional OARs that need to be protected, and desired spatial gradient of the developed distribution. As such, the highest priority was given to target coverage to gain maximum therapeutic benefit, while keeping radiation doses that additional OARs and standard OARs received to a minimum. The conformity index (CI), the new CI (nCI), and the homogeneity index (HI) were compared. Conformity index was defined as the ratio of the volume of the

Table 3. Summary of the Differences of Parameters Between the Single-Fraction Treatment Plans With and Without the Functionally Relevant Cortical and Subcortical Areas Into the Optimization Process.^{a,b}

| Parameters | Plan With Additional OARs | Plan Without Additional OARs | <i>t</i> | <i>P</i> |
|---|---------------------------|------------------------------|----------|----------|
| Maximum dose nearby functional structures and fiber tracts received | 1216.41 (309.16) cGy | 1521.69 (368.52) cGy | -6.367 | .003 |
| Mean dose nearby functional structures and fiber tracts received | 544.31 (273.67) cGy | 777.14 (508.49) cGy | -2.050 | .110 |
| Minimum dose nearby functional structures and fiber tracts received | 185.09 (190.37) cGy | 397.48 (472.17) cGy | -1.663 | .172 |
| Tumor coverage | 93.36 (2.76) | 96.31 (1.87) | -1.561 | .193 |
| No of beams | 108.40 (10.92) | 108.60 (4.16) | 0.883 | .398 |
| CI | 1.18 (0.06) | 1.17 (0.10) | 0.191 | .858 |
| nCI | 1.26 (0.08) | 1.21 (0.12) | 0.669 | .540 |
| HI | 1.36 (0.10) | 1.28 (0.08) | 1.625 | .179 |
| MU | 9338.66 (1215.22) | 8856.06 (943.18) | 1.886 | .132 |

Abbreviations: CI, conformity index; HI, homogeneity index; MU, monitor unit; nCI, new CI; OARs, organs at risk.

^aMaximum, mean, and minimum dose to nearby functional structures and fiber tracts, tumor coverage, number of beams and MUs, CI, nCI, and HI without and with the inclusion of the nearby functional structures and fiber tracts in the optimization process for the single-fraction treatment studied cases are shown.

^bThe values of tumor coverage are expressed in percentage.

Table 4. Summary of the Differences of Parameters Between the 3-Fraction Treatment Plans With and Without the Functionally Relevant Cortical and Subcortical Areas Into the Optimization Process.^{a,b}

| Parameters | Plan With Additional OARs | Plan Without Additional OARs | <i>t</i> | <i>P</i> |
|---|---------------------------|------------------------------|----------|----------|
| Maximum dose nearby functional structures and fiber tracts received | 1703.10 (442.80) cGy | 2015.26 (485.49) cGy | -4.415 | .001 |
| Mean dose nearby functional structures and fiber tracts received | 525.82 (302.66) cGy | 695.66 (386.72) cGy | -4.587 | .001 |
| Minimum dose nearby functional structures and fiber tracts received | 113.79 (115.84) cGy | 139.71 (111.24) cGy | -1.265 | .234 |
| Tumor coverage | 95.67 (2.22) | 96.77 (1.29) | -1.655 | .129 |
| No. of beams | 110.73 (15.28) | 106.91 (6.25) | 0.883 | .398 |
| CI | 1.23 (0.22) | 1.21 (0.23) | 0.993 | .344 |
| nCI | 1.29 (0.23) | 1.25 (0.24) | 1.722 | .116 |
| HI | 1.33 (0.09) | 1.23 (0.04) | 3.243 | .009 |
| MU | 18 667.86 (5013.77) | 15 923.15 (2863.44) | 3.322 | .008 |

Abbreviations: CI, conformity index; HI, homogeneity index; MU, monitor unit; nCI, new CI; OARs, organs at risk.

^aMaximum, mean, and minimum dose to nearby functional structures and fiber tracts, tumor coverage, number of beams and MUs, CI, nCI, and HI without and with the inclusion of the nearby functional structures and fiber tracts in the optimization process for the 3-fraction treatment cases are shown.

^bThe values of tumor coverage are expressed in percentage.

prescription isodose surface to the target volume that is encompassed by the prescription isodose surface; nCI was defined as the prescription isodose volume multiplied by the target volume and then divided by the target volume encompassed by the prescription isodose surface squared; HI was defined as the ratio of the maximum dose to the prescription dose.¹⁵

Statistical analysis was accomplished using the Wilcoxon-matched pairs test. The data analysis was performed using SPSS (version 17.0; SPSS Inc, Chicago, Illinois). The values are expressed as the mean (standard deviation, SD).

Results

There are significant differences between the 2 treatment plans. It showed that the maximum dose to the functional areas achieved an average 16.86% reduction when they were optimized. And the reduction of the mean dose to functional areas reached 22.71%.

According to the 2 treatment plan parameters, tumor coverage and the number of beams difference had no statistical significance. The CI and the nCI had no obvious difference.

Monitor units and HI with and without the inclusion of the nearby functional structures and fiber tracts in the optimization process have obvious difference. A detailed comparison is depicted in Tables 3 and 4.

Doses to small volumes of functional structures (range: 0.886-2.473 cm³, 8 cases) were compared alone. It shows that there are still significant differences between the 2 treatment plans (see Table 5).

Discussion

Although radiosurgery being widely adopted in the last 15 to 20 years, controlling the tumors in the intracranial area has been addressed with accurate dosimetry with various dose-shaping techniques. Despite the accuracy in depicting the target region and routine OARs, there may be a high risk of radiation

Table 5. Summary of the Differences of Parameters Between Small Volumes of Functional Structures Cases Treatment Plans With and Without the Functionally Relevant Cortical and Subcortical Areas Into the Optimization Process.^{a,b}

| Parameters | Plan With Additional OARs | Plan Without Additional OARs | <i>t</i> | <i>P</i> |
|---|---------------------------|------------------------------|----------|----------|
| Maximum dose nearby functional structures and fiber tracts received | 1392.90 (413.17) cGy | 1692.01 (466.87) cGy | -6.429 | .000 |
| Mean dose nearby functional structures and fiber tracts received | 471.23 (278.46) cGy | 705.50 (446.57) cGy | -3.260 | .014 |
| Minimum dose nearby functional structures and fiber tracts received | 174.10 (189.31) cGy | 307.27 (388.79) cGy | -1.532 | .169 |

Abbreviation: OARs, organs at risk.

^aMaximum, mean, and minimum dose to nearby functional structures and fiber tracts, with and without the inclusion of the nearby functional structures and fiber tracts in the optimization process for small volumes of functional structures cases.

^bThe values of tumor coverage are expressed in percentage.

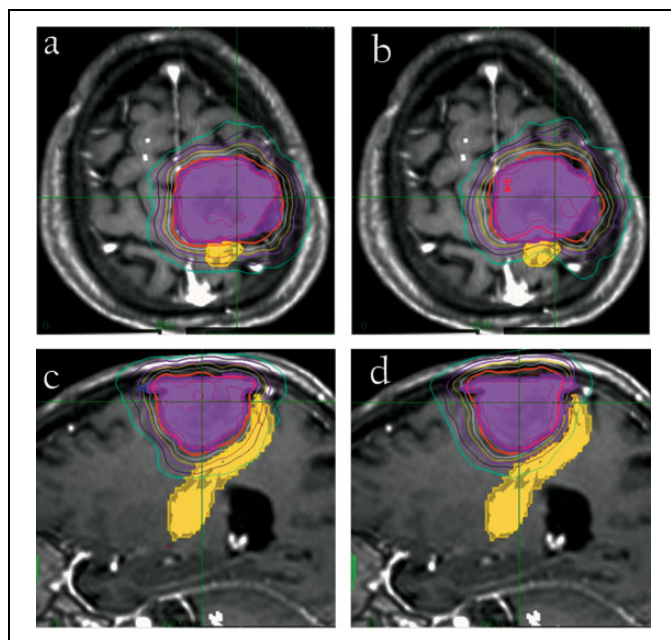


Figure 2. Treatment plans developed without (left side) and with (right side) the introduction of the pyramidal tracts in the optimization process for the meningioma case, plotted in axial and sagittal planes. This patient received 21 Gy units of radiation in 7 Gy fractions. The radiation dose to pyramidal tract is lowered from 2396.97 to 1460.96 cGy after the optimized process with pyramidal tract.

injury if the lesions are located inside critical areas. One of the clinical examples is to spare the hippocampal regions, which affects patient memory function. The change/decline in neurocognitive functions (NCFs) resulting from impaired hippocampal neurogenesis might occur after whole-brain radiation therapy. With careful dosimetric planning, the study has summarized conformal hippocampal sparing, which would provide the preservation of NCFs with radiation sparing.¹⁶ Therefore, functional structures and white matter pathways can't be recognized on conventional CT/anatomical MRI images. This invisibility makes the potential risks of critical areas nearby the lesions being exposed to high levels of radiation, which is beyond their tolerable limits for substantial side effects. Multimodality fusion is one of the most popular topics discussed in the current research of medical image processing.^{17,18} Blood

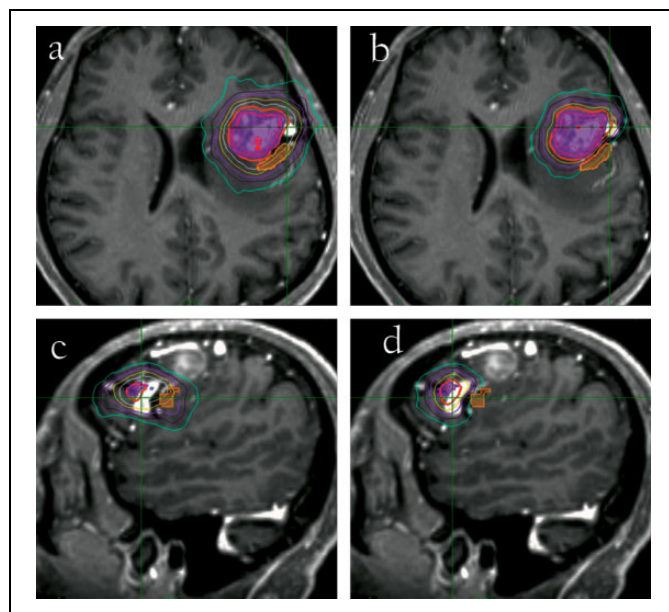


Figure 3. Treatment plans developed without (left side) and with (right side) the introduction of the language area in the optimization process for the AVM case, plotted in axial and sagittal planes. This patient received 16 Gy in single fraction. The maximum radiation dose to the language area is lowered from 1587.55 to 1273.88 cGy after the optimized process with language area. AVM indicates arteriovenous malformation.

oxygenation level-dependent fMRI can provide brain activation maps, and DTI can provide white matter tractography data. With the aid of multimodality fusion technologies, BOLD fMRI and DTI can be integrated into conventional CT/anatomical MRI images. These fused images offer us anatomical information of lesions as well as functional structures and white matter pathway information surrounding these lesions. These technologies are widely employed in surgical navigation, stereotactic brain biopsy, radiotherapy, and other fields.⁸⁻¹⁰ Conti *et al* integrated 3-D rotational angiography into CyberKnife treatment planning and achieved better 3-D understanding of the target volume and distribution of the radiation doses within the volume.¹⁹ We recently integrated BOLD fMRI and DTI tractography into our CyberKnife treatment planning with the aid of MIM software. First of all, the accuracy of image

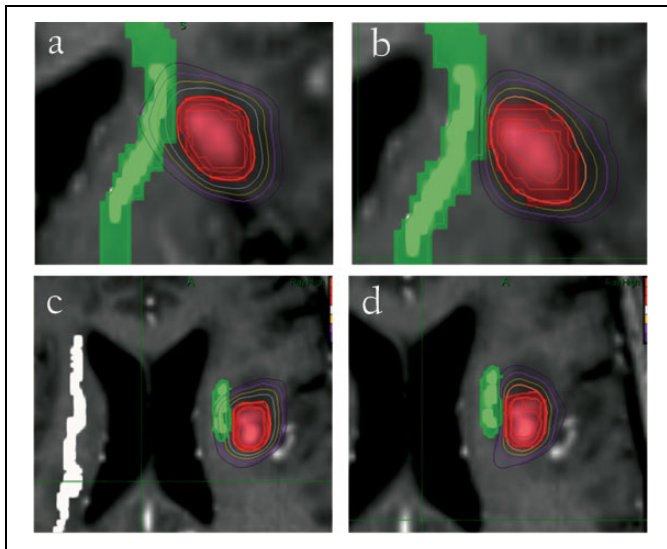


Figure 4. Treatment plans developed without (left side) and with (right side) the introduction of the pyramidal tracts in the optimization process for the brain metastases of thyroid cancer case, plotted in axial and coronal planes. The prescription dose was 13 Gy in single fraction. The radiation dose to pyramidal tract is lowered from 1350.54 to 945.08 cGy after the optimized process with pyramidal tract.

fusion plays a crucial role in this study. Registration of fMRI and DTI data sets with anatomical MRI images is mainly influenced by nonlinear geometric distortions of echo planar imaging (EPI) images that used for acquiring fMRI and DTI. We adopted parallel imaging to acquire EPI data in order to minimize this effect. And nonlinear automated shimming was performed for optimizing the homogeneity of the magnetic field.²⁰ Functionally relevant cortical and subcortical areas situated near the target were delineated using fused activation maps and tractography images. As a result, registration of fMRI and DTI data sets with anatomical MRI images to delineate the functional structures and fiber tracts as additional OARs could decrease the dose to the critical structures significantly. Conti *et al* achieved an average 17% reduction in the radiation dose to functional areas with the help of functional neuroimaging.²¹ The maximum doses delivered to critical regions could be reduced by up to 16.86% of their initial values after the integration of functional data. Risks of radiation-induced complications depend on the dose to the critical structures. In the basal ganglion AVM case, the pyramidal tract that lay within 2.5 mm of the target received a maximum dose of 2531.83 cGy when not included in the optimization process. When the pyramidal tract was brought into the optimized process as additional OARs, the maximum dose to pyramidal tract was reduced to 2225.99 cGy with careful OAR delineation. Coincidentally, in the brain metastasis from pulmonary adenocarcinoma case (the lesion located in right side of the parietal lobe), updated CyberKnife planning of the maximum radiation dose to pyramidal tract is lowered from 2489.69 to 2256.66 cGy after the optimized process with pyramidal tract. Visualization of functional structures and white matter

pathways provides sensitive functional regions, which can be easily optimized to predefined dose limit. Further, we could increase the doses to the planning target appropriately to make the treatment more effective, while ensuring that the radiation doses to nearby functional areas were within the tolerances.

In the hierarchy of priorities chosen during the plan optimization process, target coverage was given the highest priority, so that treatment plans with or without the inclusion of the fMRI data sets resulted in similar target coverage. To better observe the individual effect of the integration of fMRI and DTI tractography data into treatment plans on the dose distribution, we did not use smaller collimator sizes in the treatment plan optimization process. The same number/size of collimators was used for the treatment plan. Despite the impact of smaller collimator size on the dose distribution was small.¹⁵ We noticed that there were no significant differences in the tumor coverage, beams, CI, and nCI between the 2 groups, either single-fraction or 3-fraction treatment. It was suggested that there was no negative effect on dose distributions when the functional structures and fiber tracts were brought into the optimized process as additional OARs. Our results showed that MU and HI in the group with additional OARs were higher than that in the group without additional OARs. Due to the dose limit for the additional OARs nearby the lesions, it will be bound to cause an increase in the MU. And in our study, the values of HI are within the acceptable range of values. After all, the ultimate goal is to obtain the maximal benefits from CyberKnife treatment with precise targeting and OAR sparing.

Conclusion

Functional neuroimaging could be easily and reliably integrated into current CyberKnife treatment planning. With improved MRI techniques, functional structures of the brain and white matter fiber pathways could be marked as critical structures with the assistance of BOLD, fMRI activation maps, and DTI tractography images. Consideration of functional structures and fiber tracts during treatment planning could reduce the radiation doses to those critical structures, thereby reducing the risk of radiation-induced complications.

Authors' Note

The work has not been accepted for publication nor is concurrently under consideration elsewhere and will not be published elsewhere without the permission of the Editor and that all the authors have contributed directly to the paper.

Declaration of Conflicting Interests

The author(s) declared no potential conflicts of interest with respect to the research, authorship, and/or publication of this article.

Funding

The author(s) received no financial support for the research, authorship, and/or publication of this article.

References

1. Tamari K, Suzuki O, Hashimoto N, et al. Treatment outcomes using CyberKnife for brain metastases from lung cancer. *J Radiat Res.* 2015;56(1):151-158. doi:10.1093/jrr/rru092
2. Vlachopoulou V, Antypas C, Delis H, et al. Peripheral doses in patients undergoing Cyberknife treatment for intracranial lesions. A single centre experience. *Radiat Oncol.* 2011;6:157. doi:10.1186/1748-717X-6-157
3. Veeravagu A, Jiang B, Patil CG, et al. CyberKnife stereotactic radiosurgery for recurrent, metastatic, and residual hemangiopericytomas. *J Hematol Oncol.* 2011;4:26. doi:10.1186/1756-8722-4-26
4. Hadjipanayis CG, Levy EI, Niranjan A, et al. Stereotactic radiosurgery for motor cortex region arteriovenous malformations. *Neurosurgery.* 2001;48(1):70-76; discussion 76-77
5. Pollock BE, Gorman DA, Brown PD. Radiosurgery for arteriovenous malformations of the basal ganglia, thalamus, and brainstem. *J Neurosurg.* 2004;100(2):210-214. doi:10.3171/jns.2004.100.2.0210
6. Sasaki T, Kurita H, Saito I, et al. Arteriovenous malformations in the basal ganglia and thalamus: management and results in 101 cases. *J Neurosurg.* 1998;88(2):285-292. doi:10.3171/jns.1998.88.2.0285
7. Andrade-Souza YM, Zadeh G, Scora D, Tsao MN, Schwartz ML. Radiosurgery for basal ganglia, internal capsule, and thalamus arteriovenous malformation: clinical outcome. *Neurosurgery.* 2005;56(1):56-63; discussion 63-54
8. Krishnan AP, Asher IM, Davis D, Okunieff P, O'Dell WG. Evidence that MR diffusion tensor imaging (tractography) predicts the natural history of regional progression in patients irradiated conformally for primary brain tumors. *Int J Radiat Oncol Biol Phys.* 2008;71(5):1553-1562. doi:10.1016/j.ijrobp.2008.04.017
9. Kamada K, Todo T, Masutani Y, et al. Combined use of tractography-integrated functional neuronavigation and direct fiber stimulation. *J Neurosurg.* 2005;102(4):664-672. doi:10.3171/jns.2005.102.4.0664
10. Pirotte B, Voordecker P, Neugroschl C, et al. Combination of functional magnetic resonance imaging-guided neuronavigation and intraoperative cortical brain mapping improves targeting of motor cortex stimulation in neuropathic pain. *Neurosurgery.* 2005;56(suppl 2):344-359; discussion 344-359
11. Adler JR Jr., Chang SD, Murphy MJ, Doty J, Geis P, Hancock SL. The Cyberknife: a frameless robotic system for radiosurgery. *Stereotact Funct Neurosurg.* 1997;69(1-4 pt 2):124-128.
12. Romanelli P, Schaal DW, Adler JR. Image-guided radiosurgical ablation of intra- and extra-cranial lesions. *Technol Cancer Res Treat.* 2006;5(4):421-428.
13. Chang SD, Adler JR. Robotics and radiosurgery—the CyberKnife. *Stereotact Funct Neurosurg.* 2001;76(3-4):204-208.
14. Cui ZQ, Ling ZP, Song HF, et al. Combining pyramidal tract mapping, microscopic-based neuronavigation, and intraoperative magnetic resonance imaging improves outcome of epilepsy foci resection in the sensorimotor cortex. *Turkish Neurosurg.* 2014; 24(4):538-545. doi:10.5137/1019-5149.JTN.9517-13.0.
15. Pantelis E, Papadakis N, Verigos K, et al. Integration of functional MRI and white matter tractography in stereotactic radiosurgery clinical practice. *Int J Radiat Oncol Biol Phys.* 2010;78(1): 257-267. doi:10.1016/j.ijrobp.2009.10.064.
16. Tsai PF, Yang CC, Chuang CC, et al. Hippocampal dosimetry correlates with the change in neurocognitive function after hippocampal sparing during whole brain radiotherapy: a prospective study. *Radiat Oncol.* 2015;10:253. doi:10.1186/s13014-015-0562-x.
17. Jbabdi S, Mandonnet E, Duffau H, et al. Simulation of anisotropic growth of low-grade gliomas using diffusion tensor imaging. *Magn Reson Med.* 2005;54(3):616-624. doi:10.1002/mrm.20625.
18. Leclercq D, Duffau H, Delmaire C, et al. Comparison of diffusion tensor imaging tractography of language tracts and intraoperative subcortical stimulations. *J Neurosurg.* 2010; 112(3):503-511. doi:10.3171/2009.8.JNS09558.
19. Conti A, Pontoriero A, Farago G, et al. Integration of three-dimensional rotational angiography in radiosurgical treatment planning of cerebral arteriovenous malformations. *Int J Radiat Oncol Biol Phys.* 2011;81(3):e29-37. doi:10.1016/j.ijrobp.2010.12.024.
20. de Zwart JA, van Gelderen P, Kellman P, Duyn JH. Application of sensitivity-encoded echo-planar imaging for blood oxygen level-dependent functional brain imaging. *Magn Reson Med.* 2002; 48(6):1011-1020. doi:10.1002/mrm.10303.
21. Conti A, Pontoriero A, Ricciardi GK, et al. Integration of functional neuroimaging in CyberKnife radiosurgery: feasibility and dosimetric results. *Neurosurg Focus.* 2013;34(4):E5. doi:10.3171/2013.2.FOCUS12414.